

# Investigation of the Surface Composition by Laser Ablation/Ionization Mass Spectrometry

Peter Wurz  
Physics Institute, University of Bern,  
Sidlerstrasse 5, 3012 Bern,  
Switzerland  
peter.wurz@space.unibe.ch

Marek Tulej  
Physics Institute, University of  
Bern, Sidlerstrasse 5, 3012 Bern,  
Switzerland  
marek.tulej@space.unibe.ch

Andreas Riedo  
Physics Institute, University of  
Bern, Sidlerstrasse 5, 3012 Bern,  
Switzerland  
andreas.riedo@space.unibe.ch

Valentine Grimaudo  
Physics Institute, University of Bern,  
Sidlerstrasse 5, 3012 Bern,  
Switzerland  
valentine.grimaudo@space.unibe.ch

Rustam Lukmanov  
Physics Institute, University of  
Bern, Sidlerstrasse 5, 3012 Bern,  
Switzerland  
rustam.lukmanov@space.unibe.ch

Nicolas Thomas  
Physics Institute, University of  
Bern, Sidlerstrasse 5, 3012 Bern,  
Switzerland  
nicolas.thomas@space.unibe.ch

**Abstract**— We present a Laser Ablation Ionization Mass Spectrometer (LIMS) for the sensitive, chemical analysis of solid matter as an analytical instrument on a landed spacecraft on the Moon, as a possible application in the ARTEMIS program of NASA. Our LIMS system is compact, features simple and robust operation, and is based on current measurement capabilities of a real-size prototype system. Our LIMS instrument can be part of the payload of a rover, can be portable for field excursions of astronauts, or be part of an instrument suite at the lunar base for detailed investigations of samples collected in the field. LIMS measurements provide chemical analysis within seconds, detection of trace elements at the ppm level and below, without sample preparation to support investigations from pure scientific interest all the way to in situ resource utilization (ISRU) related tasks. The LIMS instrument is a reflectron-type time-of-flight mass spectrometer coupled to a femtosecond laser for ablation and ionization of sample material for mass spectrometric analysis of solid samples. The LIMS was originally designed for the application on Mercury surface and since then was continuously developed further for in situ research on planetary surfaces. We operated a fully functional LIMS prototype that has been operated for many years in our laboratory. It has a mass resolution up to 900, with an accuracy of the mass scale of 500 ppm, a detection limit around 10 ppb depending on mass, and a dynamic range of 8 decades, which allows for quantitative measurements of almost all elements in laser ablation mode. Furthermore, it enables the detection of complex molecules in laser desorption mode. With every laser pulse a small amount of sample material is removed, thus, when staying at the same spot the sequence of mass spectra resulting from these laser pulses can be used to derive a depth profile of the atomic composition at the sampled location, allowing, for example, to penetrate through the space weathered layer on grains and rocks to access the true chemical composition of the material. We combined our LIMS system with a high-resolution microscope camera system (MCS), which has its own multi-color sample illumination. MCS has an optical resolution of 2  $\mu\text{m}$  for detailed optical investigation of the sample. In this way, mass spectrometric analysis and imaging information are available from the exact same location on the sample. Microscope images provide characterization of a sample for context analysis and supporting mineralogical classifications. For the demonstration of performance of our miniature LIMS system, we will present exemplary studies conducted on suitable

sample materials that are relevant for in situ space exploration, that includes e.g., the identification of the mineralogy of heterogeneous samples, as well as element and isotope studies conducted on lunar and chondritic meteorites, which allows studies of in situ radio-isotope geochronology.

## TABLE OF CONTENTS

1. INTRODUCTION .....	1
2. INSTRUMENT DESCRIPTION .....	2
3. MASS SPECTROMETER PERFORMANCE .....	3
4. MICROSCOPE PERFORMANCE .....	9
5. FLIGHT INSTRUMENT DESIGN .....	9
6. CONCLUSIONS .....	11
7. ACKNOWLEDGEMENTS .....	11
REFERENCES .....	11
BIOGRAPHY .....	14

## 1. INTRODUCTION

Our research on planetary surfaces is concerned with the composition of the material at or near the surface, the regolith, the rocks, and the volatile material contained therein of which we measure the chemical, elemental, and isotope composition, at high spatial resolution, of surface material with laser-based mass spectrometry. From the recorded mass spectra we derive the local mineralogy and petrology. These data provide crucial information about physical conditions of their formation [1].

We developed two highly miniature Laser Ablation Ionization Mass Spectrometry (LIMS) instruments for in situ planetary research [2,3,4], which were originally intended for a lander on Mercury as part of the BepiColombo mission of ESA [5]. LIMS uses pulsed lasers of high intensity ( $\text{MW}/\text{cm}^2$  to  $\text{TW}/\text{cm}^2$ ) so that the material in the ablation plume is completely atomized and a large fraction of the atoms are ionized simultaneously. For almost two decades, we

continuously improved the larger of the two LIMS instruments in preparation for future landed missions for versatile use on lunar, asteroid, Mars and other planetary surfaces. Also thanks to our work, LIMS has advanced towards a true alternative for the sensitive and quantitative chemical analysis of solid materials with high spatial resolution. We achieved a performance comparable to state-of-the-art laboratory techniques, such as SIMS, LA-ICP-MS or GD-TOF-MS, see review [6, 7].

After exchanging the original ns-laser system to a fs-laser system for the laser ablation/laser ionization, the overall instrument performance was improved significantly allowing more sensitive chemical analysis, better reproducibility and improved accuracies of quantitative chemical analysis, and the calibration is more robust [8].

We recently upgraded our LIMS instrument and combined it with a microscope imaging system [9] allowing for in situ imagery of the sample at micrometer spatial resolution. The usefulness of such a combination was suggested already some time ago [1]. In 2014, we proposed such an instrument for the MarcoPolo asteroid mission [10].

## 2. INSTRUMENT DESCRIPTION

The mass analyzer of the instrument is a miniature reflectron-type time-of-flight (R-TOF) mass spectrometer located inside a vacuum chamber at pressure maintained at an operating pressure below  $10^{-7}$  mbar. The sample is located right at the entrance of the ion-optical system. With every laser pulse a small amount of sample material is ablated, about 1 pg per laser shot, with the amount depending on laser pulse energy and sample material. The ablated material is atomized, ionized and subjected to mass analysis. Positive ions produced during the laser ablation process can enter the ion optics of TOF system. The ions are accelerated and focused by an immersion lens, which collects almost all produced ions, and guides these ions onto the TOF path. After passing the drift tube the ion path is folded by an ion mirror, which also has energy and spatial focusing capabilities. The energy focusing improves the mass resolution, the spatial focusing assures that all ions are directed to the detector at the end of the drift path (see Fig. 1 for the schematics of the ion optics).

For laser ablation we currently use a pulsed laser system (Chirped Pulse Amplified (CPA), Clark-MXR Inc., USA) that generates pulses of  $\sim 190$  fs pulse width at 1 kHz laser pulse repetition rate at 258 nm wavelength. This wavelength is produced by harmonic conversion from the fundamental at 775 nm (Storc, Clark-MXR Inc., USA). The femtosecond laser beam has a Gaussian shaped cross section, both temporal and spatial. A dedicated optical system consisting of dielectric mirrors (e.g., Thorlabs Inc., USA) and beam expander (Eksma Optics, Lithuania) guides the laser pulses towards the vacuum chamber, through an entrance window, focused through the mass analyzer with a lens system installed on top of the mass analyzer, along its central axis, towards to the sample which is positioned right below the entrance optics of the analyzer. The sample surface is

remotely manipulated by a x,y,z-translation stage with micrometer positioning accuracy at the focal plane of the laser beam. The location of the focal plane is investigated once, at the beginning of the measurement campaign, by online monitoring of the recorded signal intensity and the crater size for very low pulse energies. At these laser conditions, both a clear signal and a crater are only observed when the sample surface is located at the focal point. The positioning of the focal plane is done with an accuracy of about 10  $\mu\text{m}$ . In the current arrangement the ion-optical settings transmit only positively charged species towards the detection unit, which consists of two microchannel plates (MCP's) in chevron configuration and four centrosymmetric anodic rings [11]. These anodes have different gains, and only one or all four anodes are used for the detection of the ion current depending on the study.

Each laser pulse, hence each ablated plasma plume from the sample surface, triggers the recording of a 20  $\mu\text{s}$  long time-of-flight (TOF) spectrum, corresponding to a mass range of 1 to about 700 m/z. The signal registered on the detector is recorded by a high-speed ADC data acquisition system (U5303A, Acqiris SA, Switzerland) with a sampling rate of 3.2 GS/s and a vertical range of 12 bit. To increase the dynamic range of the signal, we usually sum up multiple TOF spectra, i.e., we perform histogramming. This histogramming can already be performed directly in the data acquisition system, as well as later during the data analysis procedure, depending on the analytical needs. Depth profiling studies are the exception, where single laser pulse spectra are analyzed [12]. The extend of histogramming amounts to a compromise between mass resolution and ion transmission hence signal intensity.

Figure 1 shows a schematic drawing of the LIMS instrument, where the ion-optical system is displayed with some sample ion trajectories originating from the ablation plume from the sample, passing through the drift tube, being reflected by the ion-mirror onto the detector after passing the drift tube a

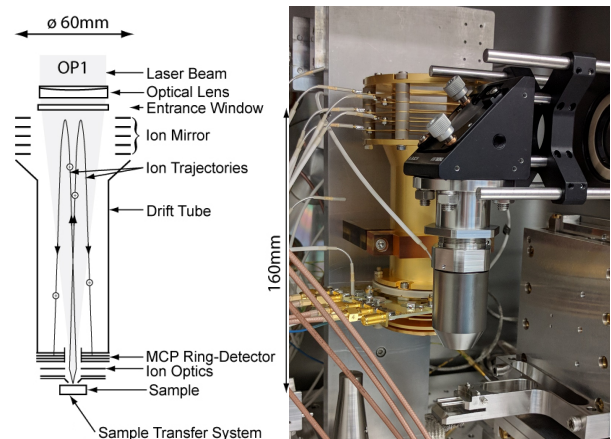


**Fig. 1: LIMS instrument: Left schematic drawing of the LIMS instrument; Right: the actual mass spectrometer (golden structure in the back) and the microscopic imaging system in front [9]. The sample is moved between the two by a translation stage with  $\mu\text{m}$  resolution and repeatability.**

second time. The schematics in Fig. 1 also show the final path of the ablation laser beam optics. The laser pulses are introduced co-axially to the ion-optical system with the last lens being located above the ion-mirror focusing the laser beam onto the sample surface while passing through the ion-optical system. Figure 1 also shows the actual mass spectrometer and the front end of the microscope imaging system. The sample is transferred between these two systems with micrometer accuracy.

### 3. MASS SPECTROMETER PERFORMANCE

We achieve comparable performance like much larger state-of-the-art laboratory instruments, such as SIMS, LA-ICP-MS or GD-TOF-MS [6], and we are among the leading groups in laser-based mass spectrometry world-wide, see a recent review [13]. The LIMS performance allowed us addressing many research questions in planetary science [e.g., 9, 14, 15, 16, 17, 18, 19] and in applied science [e.g., 12, 20, 21, 22, 23], as well as contributions to laser ablation science [e.g., 22, 28, 40].

#### Mass Range

Each laser pulse triggers a TOF spectrum. The TOF mass spectra are measured on a linear time scale  $t$  by the high-speed ADC data acquisition system, and the recording extends for a 20  $\mu$ s long TOF spectrum.

The transformation into mass scale is made with two calibration factors using the simple relation

$$m = k_0(t - t_0)^2$$

where  $m$  (u) is the mass,  $t$  (ns) denotes TOF,  $k_0$  and  $t_0$  are the calibration constants, which are determined experimentally from the TOF spectra directly. Because the values of  $k_0$  and  $t_0$  constants depend on the voltage settings of the ion optical system, they are subject to changes. The accuracy of the mass scale about 500 ppm [4]. The mass calibration can be derived from each mass spectrum individually, if necessary, as long as two peaks at TOFs  $t_1$  and  $t_2$  in the TOF spectrum can be identified as masses  $m_1$  and  $m_2$ :

$$t_0 = \frac{(\sqrt{m_1/m_2})t_2 - t_1}{(\sqrt{m_1/m_2}) - 1}$$

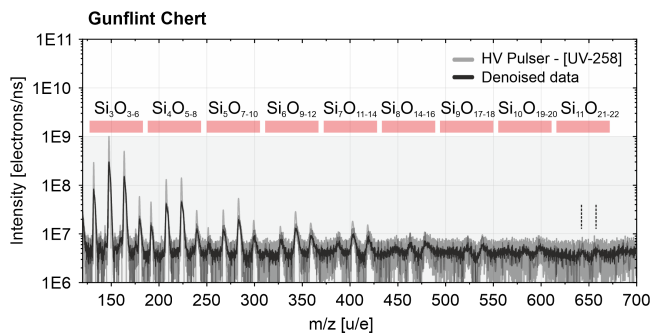


Fig. 2: High-mass section of a geological sample, a Gunflint chert, from [14].

$$k_0 = \frac{m_1}{(t_1 - t_0)^2} \quad \text{or} \quad k_0 = \frac{m_2}{(t_2 - t_0)^2}$$

This procedure allows for accurate in-flight calibration of the mass scale at any time, and it is independent of reference samples.

The constants  $k_0$  and  $t_0$  can be calculated also by using the parameters obtained by a linear regression of the flight times for elements and isotopes identified in the TOF spectrum against the square root of the attributed absolute mass values from the literature [4].

Figure 2 shows a mass spectrum from a geological sample, a Gunflint chert [14], which is a fine-grained sedimentary rock composed of microcrystalline crystals of quartz, to demonstrate the mass range. The TOF spectrum of 20  $\mu$ s duration converts to a mass range of 1 to about 700 m/z, where the larger silicon oxides,  $\text{Si}_x\text{O}_y$ , can be identified up to masses of 700 m/z.

#### Mass Resolution

The mass resolution of our LIMS instrument typically is  $m/\Delta m = 200\text{--}500$ , depending on mass, for element analysis of geological samples. The mass resolution can be raised to  $m/\Delta m \approx 900$  for isotope ratio measurements by optimizing the voltages applied to the ion optical system and the detector, as well as optimizing the laser pulse energy [24].

#### Sensitivity

Detection sensitivity is an important parameter for the chemical composition analysis, since the interesting information of a sample is often at element abundances at trace level. High sensitivity is also important for the accurate determination of isotope abundances, because many interesting isotopes are at low abundances. Competing instruments for in situ composition analysis have sensitivities at the per mil level. For example, Laser-Induced Breakdown Spectroscopy (LIBS) is used to measure the chemical composition of rocks [25, 26] aboard of the Mars Science

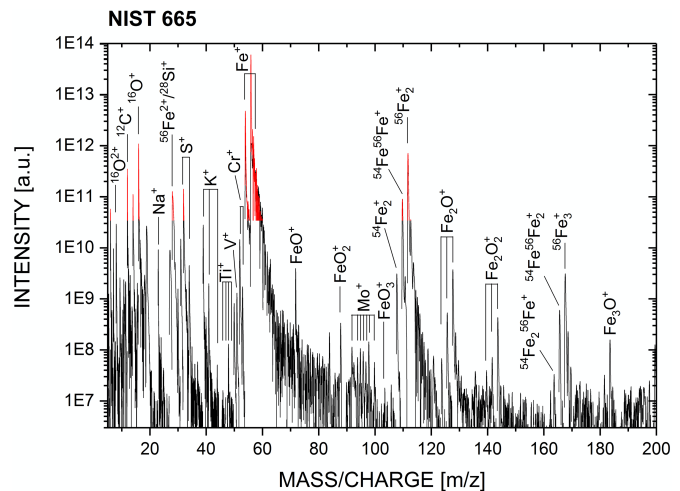


Fig. 3 Mass spectrum of a superimposed high-gain anode (black) and low-gain anode (red) signal of measurements on NIST SRM 665 reference sample [11].

Laboratory Rover Curiosity, which has a sensitivity for elements down to the percent or per mil level, depending on species. Similarly, the Alpha-Particle X-ray Spectrometer (APXS) instrument has a sensitivity for elements down to the percent or per mil level, also depending on species [27]. In comparison, with our LIMS instrument we routinely achieve a detection limit at the ppm level, and in favorable cases down to the 10 ppb level [10].

A crucial part of the good sensitivity and mass resolution of our LIMS instrument is the MCP detector system with 4 separate anodes, which allows recording up to 4 mass spectra simultaneously at different gain levels. We developed a special impedance-matched strip-line technology for the anode of the detector for the signal pick-up, with single-ion pulses of only 250 ps width [11]. Combining measurements of 2, 3 or all 4 anodes at different gains we accomplished a dynamic range of almost 8 orders of magnitude. Figure 3 is showing a measurement on a NIST SRM 665 sample using the combination of two detector channels.

### Detection of Molecules

By operating the laser at lower pulse intensities, in the range of 10 – 100 MW/cm<sup>-2</sup>, we perform measurements in the laser desorption mode, instead of the laser ablation mode. Laser desorption allows for the detection of complex molecules present on the surface, and even to obtain some structural information from these molecules [7, 10, 20]. By combining laser ablation and laser desorption modes during depth profiling at high spatial resolution, it was possible to verify complex molecular interaction pathways that occur at grain boundary sides inside the sample [28]. Figure 4 shows two laser desorption mass spectra recorded with our LIMS instrument from two complex chemical substances used in the Cu plating processes in the semiconductor industry [7]. The bottom panel shows the monomer peaks of a co-polymer of imidazole and epichlorohydrin (IMEP polymer) and the top panel shows the fragment peaks of bis-sodium-sulfopropylsulfide (the suppressor ensemble). From the fragment peaks a more complex molecular structure can be

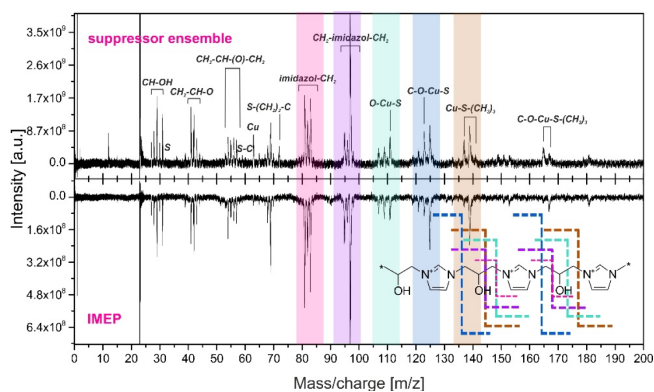


**Fig. 4: Laser desorption mass spectra of the precipitated suppressor ensemble (top spectrum) and the pristine IMEP polymer (bottom spectrum) [7]. Dashed lines in the schematics of the IMEP molecules indicate fragments observed in the mass spectra shown with a colored background of same color.**

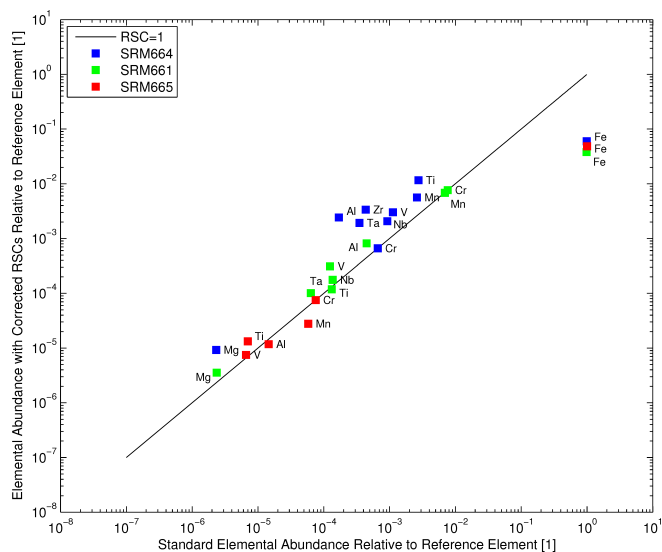


**Fig. 5: Comparison of the measured abundances by our LIMS to the certified values. The Fe measurements are low, because the <sup>56</sup>Fe signal is saturated in this detector channel.**

identified in the mass spectra (see Fig. 4, where the IMEP fragments are indicated by colored background). The presence of these molecules indicates the occurrence of a specific chemical interaction between different substances (imidazole, thiolate-related fragments and Cu) during the electrolytical reaction [6].

### Quantitative Measurements of Element Abundances

The quantitative measurement of the abundance of elements in a sample is another important parameter for composition analysis. We perform quantitative measurements of almost all elements in laser ablation mode. The accuracy of the quantitative determination of element abundances is verified against references samples, either analyzing metallic samples from NIST, e.g., SRM 661, SRM 664, and SRM 665 [8, 10], or analyzing geological standards [29]. Figure 5 shows a comparison of the measured abundances by our LIMS to the certified values by NIST for the more abundant elements. Ideally, all points would lie on the line with slope 1. From the deviations to this line we derive the calibrations constants for LIMS. Recently, we developed an analysis procedure where the calibration for mineralogical samples can be accomplished without relying on separate standard samples [30]. This is of particular importance in case a specific reference sample is required but not available during a space exploration mission.

In a composition study of Cu-Sn-Pb ternary alloys we compared our results with analyses by ICP-CRI-MS and LA-ICP-MS instruments and found that the three independent measurements agreed well within error [21]. Table 1 shows the comparison between our LIMS measurements and two ICP-MS analyses. Although the two ICP-MS studies quote smaller errors than we can assign to our LIMS measurements, it turns out that the differences between the two independent

ICP-MS measurements are larger than their quoted error bars using aliquots of the sample [21].

### Isotope Measurements

Accurate isotope abundance determination provides valuable data in planetary science about processes modifying matter and of their timing. Probably the single most important application of isotope measurement would be the determination of the absolute age, for example dating the rocks in the South Pole Aitken Basin on the Moon. Radiometric dating of rocks (finding ages using the abundances of radioactive isotopes and their decay products) is the most precise and reliable way to determine quantitative planetary chronology [1]. Currently, there are three different concepts proposed for in situ dating of planetary matter: the Sr-Rb method [31], the K-Ar method [32, 33], which was used on the Curiosity rover [34], and the lead isotope method we plan to use [8], for which a LIMS instrument is necessary.

We determined the accuracy of isotope abundance measurements as function of the abundance of species using NIST steel reference samples and found that the accuracy degrades with lower abundance, as expected [10, 24], but the accuracy still is sufficient for in situ planetary research for species at the 10 ppm level. Figure 6 shows the correlation between the abundance of an isotope and the accuracy with which this isotope abundance can be measured with our LIMS instrument. After the improvement of the laser optical system, which resulted in a smaller laser focus on the sample, we find that the accuracies of the measured isotopes are better than at the percent-level, the isotope abundances have to be larger than about 2 ppm, and at 100 ppb isotope abundances a relative accuracy of 4% is measured.

For dating we decided to investigate the Pb-Pb isotope technique because that can be done using only the Pb isotopes, which removes the need to establish the element sensitivities of the instrument with high accuracies. The difficulty in this measurement is the low abundance of Pb in typical planetological samples. To assess the potential of Pb dating we performed measurements with a NIST Pb reference sample (NIST SRM 981), with Galena samples, and a NIST iron sample with 66 ppb lead to derive the accuracies for the abundances of the Pb isotopes. By optimizing the laser fluence for ablation and the data acquisition procedure for isotope measurements we reached good accuracy. For galena samples we achieved accuracies at the per mil level and better, which are comparable to those values derived from TIMS measurements conducted on the same sample material [24].

**Table 1: Summary of composition measurements for three Cu-Sn-Pb alloy samples obtained by LMS, ICP-CRI-MS and LA-ICP-MS techniques. Abundances and errors are given in wt% [21].**

		DIN 1716	LMS	ICP-MS	LA-ICP-MS
<b>CuSn10Pb10</b>	Cu	78.0-82.0	78.61 ± 11.87	82.26 ± 4.13	76.99 ± 0.75
	Sn	9.0-11.0	9.94 ± 2.45	6.69 ± 0.79	10.91 ± 0.19
	Pb	8.0-11.0	12.25 ± 3.28	11.13 ± 0.63	8.56 ± 0.47
<b>CuSn7Pb15</b>	Cu	75.0-79.0	77.93 ± 11.77	75.55 ± 3.73	70.67 ± 1.03
	Sn	7.0-9.0	5.65 ± 1.39	6.56 ± 0.40	7.30 ± 0.06
	Pb	13.0-17.0	14.89 ± 3.99	19.45 ± 0.57	18.42 ± 1.04
<b>CuSn5Pb20</b>	Cu	69.0-76.0	76.37 ± 11.53	75.63 ± 3.39	74.94 ± 0.68
	Sn	4.0-6.0	5.99 ± 1.48	7.08 ± 0.73	6.92 ± 0.11
	Pb	18.0-23.0	15.63 ± 4.19	20.59 ± 1.25	16.59 ± 0.62

To estimate the expected accuracy of our instrument for lead dating we used the  $^{207}\text{Pb}/^{206}\text{Pb}$  data from monazite grains from Paleoproterozoic metamorphic rocks from West Greenland [35], which have a high Pb abundance ranging from 100's to 1000's ppm. We assume a constant  $^{207}\text{Pb}/^{206}\text{Pb}$  ratio of 0.11261 in these estimates. Since the concentrations of radiogenic elements in the lunar soil are in the ppm range [36], we have to look for mineral inclusions where these are enriched. For an estimate, we used data for zircon grains in lunar KREEP, which are highly abundant in U, Th, Pb in the range of 10's to 100's ppm [37]. Using these data and the LIMS isotope accuracies (see Fig. 6), we calculate for the estimated uncertainty for in situ dating using our LIMS system an uncertainty of about ±10 million years for the age determination by LIMS for a realistic lunar mineral (see Fig. 7). Such accuracy will be scientifically very valuable when LIMS is used on the lunar surface investigating element and isotope composition of surface material, for example in the South Pole Aitken basin.

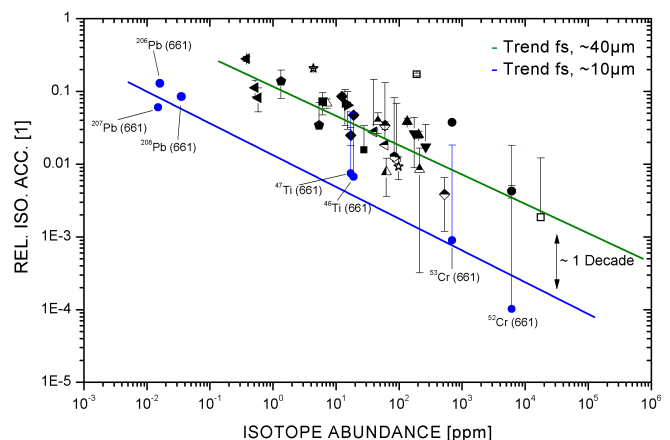


**Fig. 6: Correlation between measured accuracy of isotope ratios determined from mass spectra and their abundance in the NIST SRM 661 sample [from 10]. Black points indicate the initial laser optics setup, blue points are for an improved setup.**

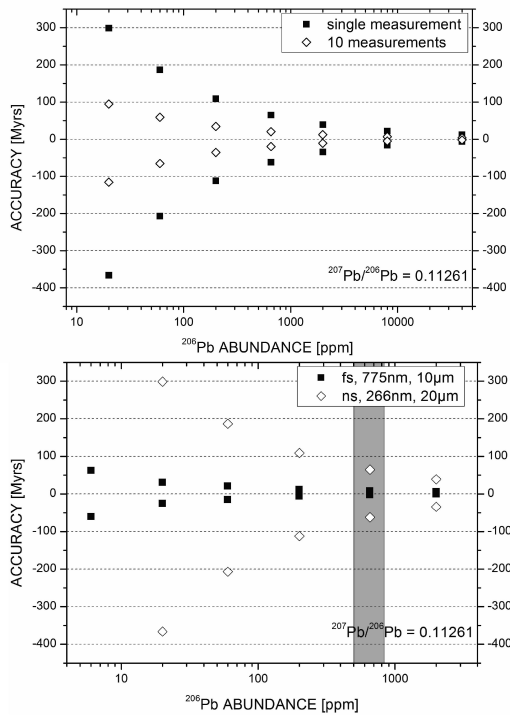


**Fig. 7: Top: Correlation between  $^{207}\text{Pb}$  and  $^{206}\text{Pb}$  abundances and accuracies for  $^{207}\text{Pb}/^{206}\text{Pb}$  dating in lunar zircon grains [24]. Filled squares give the estimated age uncertainty based on a single measurement of one grain, open diamonds the estimated age uncertainty by assuming 10 measurements of different grains, all having the same age. Bottom: comparison of dating accuracies for fs- and ns-laser system.**

In another investigation, involving isotope measurements, we studied samples that were collected from the slow-spreading Mid-Atlantic Ridge at a depth of 27 m below the seafloor during the Ocean Drilling Program Leg 209 [37]. It contains aragonite veins hosted in serpentinized harzburgite. We found microscopic structures in this sample resembling fossils both morphologically and in their chemical composition [15]. An interesting, yet challenging, goal for the investigation of these samples was to derive the Ni isotope abundances from microscopic structures, possibly methanogens. Ni is part of enzymes of these methanogens,

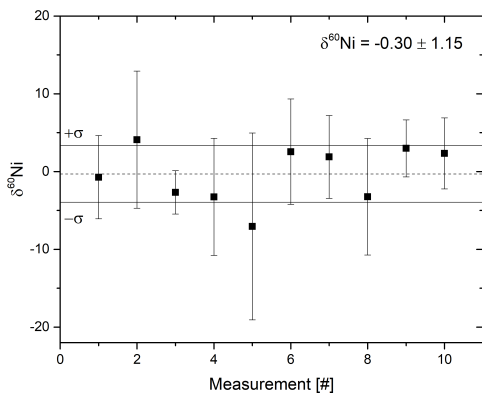


**Fig. 8: Measurement of  $\delta^{60}\text{Ni}$  isotope values on a Trevorite mineral standard with LIMS [17].**

and the light Ni isotopes will enrich in these life forms. There was a chemosynthetic dominated biosphere including methanogenesis before the great oxidation event, which changed to a photosynthetic dominated biosphere afterwards. Since the methanogens require Ni for their survival, the composition of Ni isotopes in the sample can be indicative of fossils of that time, and perhaps of similar fossils on Mars.

**Table 2: Compilation of  $\delta^{60}\text{Ni}$  measurements [16].**

Sample	$\delta^{60}\text{Ni}$
Ni metal standard (1 <sup>st</sup> run)	$-0.11 \pm 0.45$
Ni metal standard (2 <sup>nd</sup> run)	$+0.47 \pm 0.68$
Trevorite (1 <sup>st</sup> run)	$-0.02 \pm 0.91$
Trevorite (2 <sup>nd</sup> run)	$-0.30 \pm 1.15$
Stromatolites	$-4.77 \pm 1.74$
Filaments	$-3.32 \pm 0.81$

Figure 8 shows several LIMS measurements of the  $^{60}\text{Ni}/^{58}\text{Ni}$  isotope ratio for a Trevorite mineral reference sample, a rare nickel iron oxide mineral belonging to the spinel group [17].

Comparisons of the  $\delta^{60}\text{Ni}$  isotope measurements with the Ni standard NIST SRM 986 and the Trevorite mineral show the sufficient intrinsic accuracy in the Ni isotope measurement of about 1 per mil using our LIMS instrument (see Fig. 8). Because of the high spatial resolution of our LIMS system, we can investigate the microscopic fossils of stromatolite and filament embedded in the aragonite veins individually. We find that the  $\delta^{60}\text{Ni}$  isotope values show that light isotopes are enriched in fossilized microorganisms in basalts (see Table 2). In addition, we measured abundances of many trace elements such as O, Mg, Si, Mn, Co, S, C, Fe and Ni providing the mineralogical context and environmental background of the embedded fossils.

#### *Spatially Resolved Measurements*

Since most planetary samples are highly spatially heterogeneous, it is necessary to perform measurements of the chemical composition on small spots commensurate with the typical grain size of the object. Mostly a spatial resolution of 10–20  $\mu\text{m}$  is used, which is given by the laser spot size on the sample in LIMS. With our LIMS laser system we can focus the laser beam down to  $\varnothing 5 \mu\text{m}$ , which defines the best spatial resolution on a sample we can accomplish. To address the heterogeneity of typical mineralogical samples we perform analyses in 1D (depth profiles), 2D (chemical maps), and full 3D of a sample (3D resolved bulk analysis).

*1D Analysis*— Since the laser continuously removes material from the surface, the sequence of mass spectra from a sampled spot can be used to derive a depth profile of the atomic composition at the sampled location [11, 40]. We find that the obtained sampling in depth is in steps of less than 1 nm, with the step size being of course a function of applied laser intensity [12]. The high-resolution depth profiling measurements with LIMS of e.g. electrochemically deposited Cu films produced in the semiconductor technology have

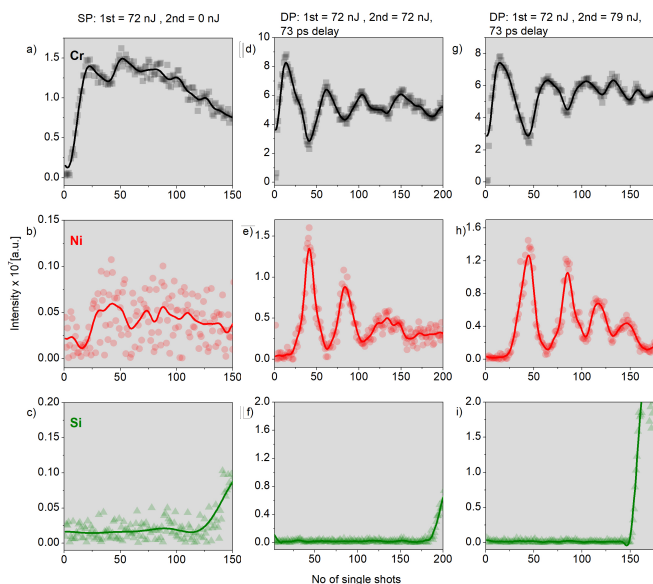


**Fig. 9: Comparison of a single pulse (SP) (A-C), double pulse (DP) with both pulses at the same energy (72 nJ) and ~73 ps delay (D-F), and DP with first pulse at 72 nJ, second pulse at 79 nJ, and 73 ps delay (G-I). Top, middle and bottom panels describe the recorded depth profiles of Cr, Ni and Si, respectively [22].**

shown the presence of complex organic contaminants located at grain boundaries [12, 20]. When drilling through the grain boundary in the course of the depth profile, we observe a sharp increase and subsequent decrease of the C, N and O contaminant signals which is in phase and is anti-correlated with the Cu signal. Compared to earlier SIMS measurements our LIMS measurements allow for element quantification, which SIMS cannot provide, and show much better depth resolution than standard SIMS instruments. We also recorded detailed depth profiles for Cu-Sn-Pb alloys, which showed large, however unexpected, chemical heterogeneity of these alloys on  $\mu\text{m}$ -scales [21].

A recent example for a 1D study is our investigation of the NIST SRM 2135c depth profiling reference standard, which has alternating layers of Cr and Ni (5 Cr layers, and 4 Ni layers) with nominal layer of thicknesses of 57 nm and 56 nm for Cr and Ni, respectively [22]. In this study we compared LIMS measurements using single pulse and double pulse methods, with the latter showing clear advantages for the depth resolution, which can be even improved by optimizing the energies of the first and second laser pulse (see Fig. 9). In the double pulse methods two co-axial laser pulses with a time difference of a few tens of ps are applied instead of one laser pulse, where the first laser pulse is mainly responsible for the laser ablation of material from the surface and the second laser pulse is mainly responsible for the ionization of particles in the ablated plume [41]. We obtain mean depth resolutions of ~37 and ~30 nm for the Cr and Ni layers, respectively, which is better than that of a state-of-the-art LA-ICP-MS instrument of the same sample [42].

**2D Analysis**—Since many planetary samples are highly heterogeneous on small spatial scales, it is necessary to

perform the measurements of the chemical composition on small spots that are commensurate with the typical grain size of the object. We compile two-dimensional composition maps of the sample surface by an array of closely-spaced ablation spots on the surface. We have completed such investigations on a piece of the Allende meteorite, a carbonaceous chondrite, where good agreement with other determinations of the chemical and mineralogical composition was achieved [19].

For the 2D analysis of sample surfaces we developed a dedicated analysis method [43] and applied it for our investigations of fossils in geological samples. Figure 10 shows element maps for  $^1\text{H}$  and  $^{12}\text{C}$  of the Gunflint sample, fossils of microbial life of almost 2 billion years ago; maps for many other elements are available [14, 15]. The different areas of the host mineral and the microbial fossils can be clearly identified from their chemical composition.

**3D Analysis**—The top surface of planetary material (soil, regolith, rocks, ...), the visible surface, is most often severely affected by weathering processes, e.g., solar wind, impact cratering, fluids, tectonics, volcanic activity, biological activity. These weathering processes affect the chemical composition and mineralogical appearance of the surface. Therefore, it is necessary to measure the unaltered material below the weathered surface. The weathering of the surface is a problem for remote sensing investigations using ultraviolet, visible, and infrared spectroscopy, which receive their information only from the uppermost surface, the weathered surface, and not from the actual surface material [44]. This is known as the “astronomers’ color problem” [45]. The Hayabusa mission of the Japanese Space Agency brought about 1500 micrometer-sized grains from the asteroid Itokawa to Earth. Their composition analysis clearly showed that the true mineral identity of a grain was masked by a weathering layer on its surface [46] and is therefore not accessible to remote sensing instrumentation. Below the

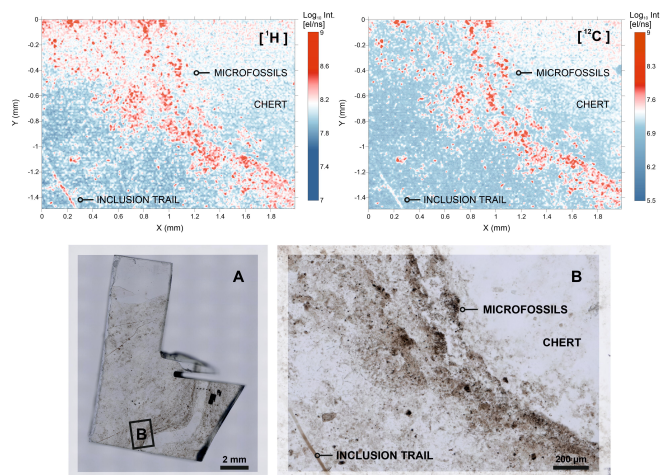


**Fig. 10: Top panels: Intensity maps of the  $^1\text{H}$  and  $^{12}\text{C}$ . Red areas correspond to the intense signal from the microfossils and blue areas to the lower intensities from the surrounding chert. Lower panels: optical images of the whole sample (left), and detail of the investigated area (right) [adapted from 15].**

weathered surface, the composition of these grains was identical to those of thermally metamorphosed LL chondrites [46]. Similar weathered surfaces have been observed routinely in grains from the lunar regolith [48, 49]. On the Mars Exploration Rovers (MER) there is a Rock Abrasion Tool (RAT) to remove the weathered surface from rocks on the Martian surface. LIMS, having a laser that can drill into mineralogical samples close to 100  $\mu\text{m}$ , removes this analytical problem without additional sample preparation steps.

An example of our recent analysis in 3D is the study of SnAg solder bumps for the semiconductor industry [23]. On the solder bumps we measured quantitatively the composition of the SnAg alloy, also in very good agreement with ICP-MS studies, but with sub- $\mu\text{m}$  spatial resolution by our LIMS instrument. We also demonstrated the Ag heterogeneity, an undesired feature in solder bumps, and we measured the amounts of chemical contaminations resulting from the plating process, e.g. Cl, C, S, Ti, and their 3D distribution. Figure 12, top row, shows the depth profiles for the two main components Ag and Sn, and for the impurities O, S, and C. As can be seen, the desired SnAg mixing ratio is only achieved further inside the solder bump, after about 1  $\mu\text{m}$  depth, but not at the surface. In addition, a significant amount of impurities, originating from the electrochemical deposition process, is present in the solder bumps, with their abundance decreasing only slowly with depth. Elaboration of matrix-matched RSC values for Sn and Ag using a certified reference material (BCS-CRM No. 347, BAS Ltd., U.K.) allowed for a very accurate quantification of the metallic phases of the alloy. The depth profile showed a severe depletion of Ag on the surface, while the LIMS-based bulk quantification of the Ag content in the alloy matrix is in excellent agreement with results from the well-established ICP-MS technique. From the 3D data presented in the five lower panels of Fig. 12 we observe, in addition, the heterogeneous distribution of Ag in the solder bump with very localized Ag clusters, as well as the heterogeneous distribution of the impurities. These data show that the 3D composition analysis at these microscopic scales adds important composition information of these features (see Fig.

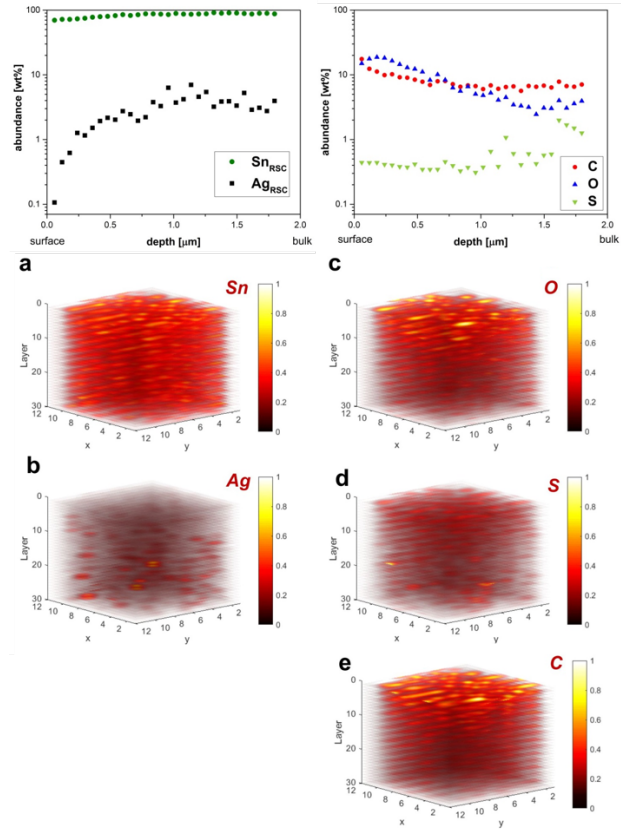


**Fig. 12: Signal intensity distribution of Sn, Ag, and the most relevant organic contaminants C, O, and S within the surface and early bulk region of the SnAg solder bump analyzed by the 2D layer binning approach. Top row: depth profiles (1D), bottom panels: 3D composition. Differences in the alloy homogeneity, SnAg, and the spatial distribution of individual organic plating bath constituents (C, O, S) are apparent. Data have been normalized to the maximum signal intensity for this representation [23].**

12) and are of particular importance to obtain a deepened understanding of the additive-assisted SnAg plating process, which to date is still a topic of research, and to which our

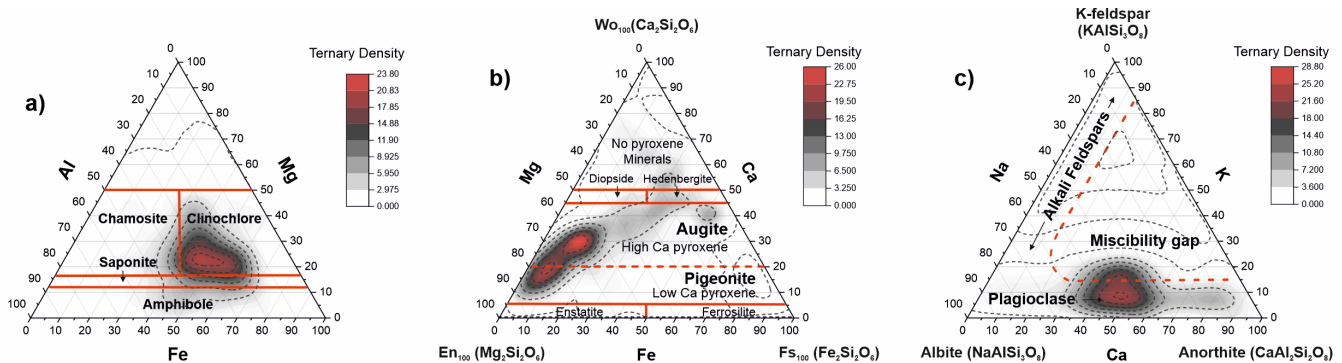


**Fig. 11: Ternary plots of the elements relevant to chlorite and feldspar groups [30]. (a): The correlation of the Al, Mg, and Fe abundances showing characteristic regions for various minerals of the chlorite group; (b): The correlation between the Mg, Fe, and Ca abundance ratios indicating presence of magnesium augite and pigeonite in the sample material; (c): The correlation diagram of the Ca, K, and Na elements indicating presence of the plagioclase feldspars in the inclusion material.**

LIMS measurements provided unique contributions to address this knowledge gap [23].

#### Determination of Mineralogy

From the element composition of an investigated location on

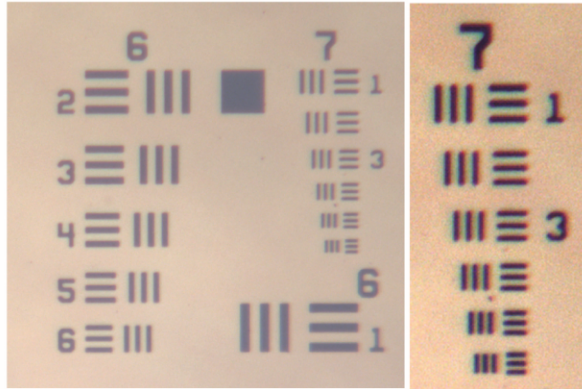


**Fig. 13: Detail of the U.S. Air Force 1951 resolution test target recorded with the microscope system (left panel: real contrast; right panel: corrected contrast). The smallest line grid has a spacing of 2.19  $\mu\text{m}$  and can be clearly resolved.**

the sample, we derive the local mineralogy. We have done that successfully for the Allende meteorite [20], for terrestrial geological standards [50], and for the lunar meteorite Sayl al Uhamir 169, a rock from the Imbrium impact basin on the Moon [51], which allowed for the separate analysis of the mineral phases.

We derived the mineralogy for Sayl al Uhamir 169, where we studied the impact-melted breccia (KREEP rich lithology), the regolith breccia, and in particular zircon inclusions [19]. In a large zircon inclusion we measured the abundance of rare earth elements from which the U-Pb age of the sample was determined as  $(3520 \pm 130) \cdot 10^6$  years. Moreover, from the Ti content in the zircon we derived the crystallization temperature of  $1180 \pm 100$  K [19].

An example of the derived mineralogy is shown in Fig. 11 for mineralogical inclusions embedded in amygdale calcium carbonate [30]. Here we present the abundances in a microscopic inclusion for key elements for chlorite and feldspar groups in a ternary plot, which typically is used to identify the mineralogical context in the analyzed sample with the minimum number of chemical species necessary to describe the composition.

#### 4. MICROSCOPE PERFORMANCE

We combined our LIMS instrument with a microscope imaging system [9], which is shown in Fig. 1. The microscope images allow to precisely target locations of interest on the sample, as well as to record complementary information of the sample surface. The usefulness of such a combination was suggested already some time ago [1], and we proposed the combination of LIMS and a microscope as the CAMAM

experiment already in an earlier proposal for in situ investigation of an asteroid [10].

Prior to the LIMS measurements, the sample surface is inspected by the in situ microscope-camera system to identify the measurement locations and to ensure overlapping of the laser spot with the defined areas of interest on the sample [9]. The overlap of the laser spot with the features on the sample surface can be made with approximately 2  $\mu\text{m}$  accuracy. The optical resolution of the microscope is about 2  $\mu\text{m}$ , commensurate with the needs for imaging mineralogical samples, which is shown in Fig. 13.

The sample can be moved with an x-y-z translation stage with respect to the laser beam focus (and entrance of the mass spectrometer). The movements in x- and y-direction are necessary for the 2D scans of the sample surface by LIMS. The movement in z-direction is to place the sample surface in the focus location of the laser beam, and of the microscope. The movement in z-direction can also be used to establish 3D images of the sample surface by the microscope from a sequence of images at difference distances to the sample, since the depth-of-field of the microscope is very small. Because the surface of a natural untreated sample is likely not flat on micrometer scales, the 3D image is helpful in adapting to the actual topography of the sample surface. A 3D microscope image compiled from such a sequence of images is shown in Fig. 14 for an untreated sample of the Mid-Atlantic Ridge (as discussed above, and in [17]) where a cliff of about 100  $\mu\text{m}$  height is imaged. Also craters from the LIMS analysis are visible on the upper edge of the cliff. Using the microscope, the successful placement of such an ablation spot onto an interesting microscopic feature can be verified, for example on a possible fossil.

#### 5. FLIGHT INSTRUMENT DESIGN

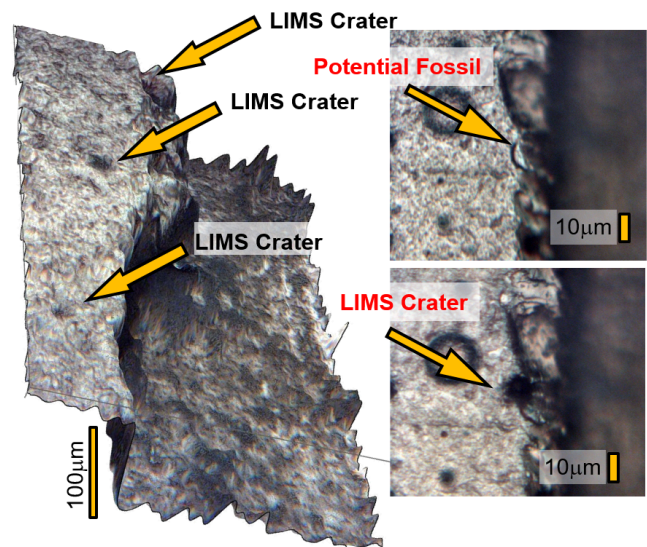


**Fig. 14: Left: 3D image of a Mid-Atlantic Ridge sample [17] with a cliff of 100  $\mu\text{m}$  height where locations of LIMS ablation craters are indicated. Right: Top view of sample with a potential fossil, before and after our LIMS analysis.**

For the proposed MarcoPolo mission of ESA we developed the design of a combined instrument, the CAMAM instrument (see Fig. 16), comprising a LIMS system and a microscope-camera system (MCS), for in situ investigation of planetary materials [11]. CAMAM is based on our LIMS instrument and the microscope discussed above, it weighs about 4.8 kg and operates at a power of 11.8 W. The performance and capability to conduct morphological, mineralogical and chemical investigations of rock or regolith/soil samples were demonstrated on prototypes. Optical analysis leads to visualization of the morphology of sample surfaces and provides clues as to the mineralogical composition. With the help of MCS, the chemical composition of the sample surface at several well-defined locations could be investigated by LIMS. The element and isotope composition will be derived from the mass spectrometric analysis to constrain mineralogical context by means of major element composition. Additionally, trace elements with concentrations below the ppm abundance level will be measured. Also, isotope abundances can be measured with accuracies at the per mil level for all major elements. In addition to addressing scientific questions relating to isotopes, the isotope abundances will be helping to resolve isobaric interference arising from polyatomic compounds. The accuracy of the isotope ratio measurements is sufficiently high to investigate isotope fractionation of a number of elements. This is of importance in the investigation of formation processes and determination of the conditions at which materials were formed.

The major challenge for the flight implementation of CAMAM and any other LIMS system is the laser system itself. One possibility are micro-chip lasers from e.g., the company Bright Solutions Srl. (Cura Carpignano, Italy), which provide passively Q-switched Nd:YAG lasers that are commercially available, even for space flight. The micro-chip lasers output ns laser pulses at the fundamental wavelength of 1064 nm, or upconverted to shorter wavelengths (higher harmonics: 532 nm, 355 nm, or 266 nm) with pulse energies of  $\mu\text{J}$  to tens of  $\mu\text{J}$  (e.g., model SB1-532-40-0.1, providing pulse energies at the level of 40  $\mu\text{J}$  at a

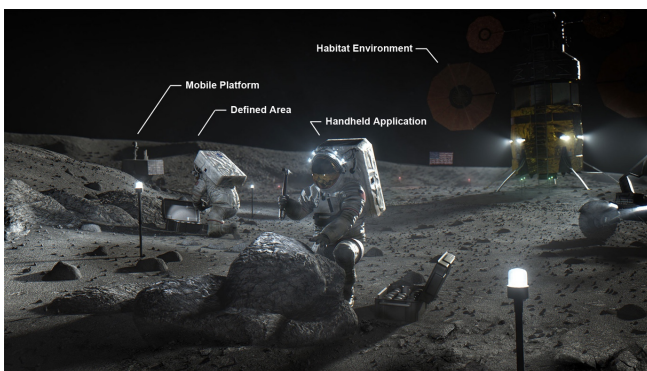


**Fig. 15: Depending on the task, instrumentation may be operated in different environments that include instruments operated in the habitat, in a predefined area, on a mobile platform, and directly in situ by the Astronaut via handheld tools. Image adapted and from NASA.**

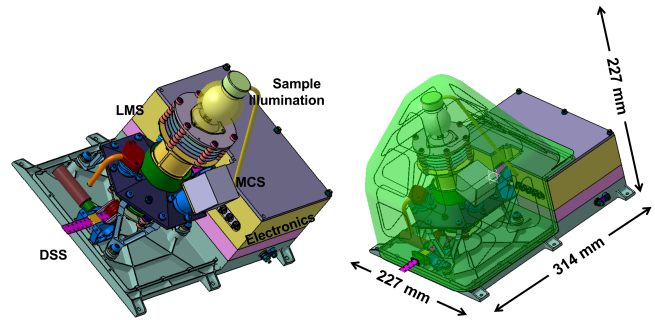


**Fig. 16: Left: Schematic diagram of the CAMAM instrument suite [10]. LIMS and MCS are aligned to allow for complementary measurements of the same sampling point. A sample is delivered to the sampling point by a sample introduction system; here, a particle trap mechanism is shown. The electronic systems are located in the electronics box. Right: CAMAM instrument suite with its protective cover.**

repetition rate of 100 Hz and wavelength of 532 nm). A micro-chip laser system was already used in the first LIMS system we built for space research [2, 3].

However, we know that fs lasers provide superior quantitative results (improved stoichiometry, cleaner material ablation, increased ionization efficiency). To be compatible with the demands of space flight only an all-fiber realization of the fs laser is feasible. All-fiber means that the laser beam is guided always inside optical fibers and there are no free-space sections of laser propagation. This has the advantage that there is no need of optical realignment and thus an all-fiber laser is inherently more robust and needs much less technical maintenance compared to bulk systems. All-fiber fs laser systems are commercially available for the laboratory, e.g., model Satsuma from the European company Amplitude, France, and flight designs can be derived from these.

In the framework of the Artemis mission of NASA we consider our LIMS system as a valuable instrument that may support the Astronauts in their field work, in what manner depends on the environments they could be deployed throughout the mission. Different major application environments were identified for employing our LIMS instrument, including i) habitat-based instrumentation, ii) instrumentation that operates remote, in a predefined, yet interesting lunar area, iii) applied on a mobile platform (e.g. the rover of the astronauts), and iv) as a handheld instrument. These application environments are illustrated in Fig. 15 and are briefly discussed below.

Heavier and potentially much more complex instrumentation can be deployed by the two Astronauts inside the lunar habitat since the possibilities for instrument manipulation by the operators without the spacesuits is comparable to a terrestrial laboratory situation. Moreover, in the habitat environment, more resources such as power and space will likely be available. On a mobile platform these resources are more limited and more compact instrumentation are required.

But the mobile platform can be brought to an interesting lunar area, which allows the astronauts to e.g., utilize the instrumentation more efficiently with local materials to be analyzed immediately at the field location, instead of bringing everything back to the laboratory in the habitat. Comparable is the pre-defined lunar area where an astronaut can install the instrument. The astronaut can utilize the instrument, if required, with one or more samples and the instrument is conducting the sample analysis autonomously, perhaps overnight. The most challenging setting is definitely the case of a handheld instrument. In such a scenario the instrument needs to be highly portable (light weight design), using low power, and very simple in operation. Simple Yes/No answers to questions like “Is lead at concentration X present” maybe provided by the instrument.

The presented LIMS system can be deployed in all the four scenarios. It provides with every laser shot applied to the target of interest the chemical composition (elements and isotopes). Nevertheless, and depending on the scenario where the LIMS system will be deployed, the instrument needs to be adapted to the specific case. The handheld case is also challenging from mechanical and also operation perspective. The measurement by a LIMS system is very fast, because single laser shot onto the sample already gives a mass spectrum with about 3 decades of dynamic range. Thus, the astronaut just needs to point the handheld LIMS system onto the sample to get an immediate answer on the chemical composition of the investigated location. Currently a study is ongoing for LIMS application in the different scenarios and provide a more profound discussion in which scenario the LIMS system can provide the best technical and scientific return [52]. Moreover, the environment will define which laser system to be integrated to the mass analyzer that is the most suitable for the task.

## 6. CONCLUSIONS

We described our work on laser-based mass spectrometry, in particular our LIMS instrument prototype designed for in situ planetary research. This instrument is complemented by a powerful microscope system for complementary information of the sample under investigation. The combination of these two units will allow to address many questions ranging from pure science, applied science, context information, all the way to In Situ Resource Utilization (ISRU) on the lunar surface. The instrument will provide element and isotope abundance information, basic data for many questions to be asked of the available material at the habitat. From these data the mineralogy of the material can be derived, which might be important in the search for building material for larger structures. Moreover, analysis of molecules present on the surface is possible if used in laser desorption mode, which might be important for the search of consumables (e.g. water).

## 7. ACKNOWLEDGEMENTS

The financial support by the Swiss National Science Foundation is gratefully acknowledged.

## REFERENCES

- [1] C. Meyer, A.H. Treiman, and T. Kostiuk, Planetary Surface Instruments Workshop, *LPI Technical Report*, 95-05 (1995), 118pp.
- [2] Rohner, U., J. Whitby, and P. Wurz, (2003) *Meas. Sci. Technol.*, 14, 2159–2164.
- [3] Rohner, U., J. Whitby, P. Wurz, and S. Barabash, A highly miniaturised laser ablation time-of-flight mass spectrometer for planetary rover, *Rev. Sci. Instr.*, 75(5), (2004), 1314–1322.
- [4] A. Riedo, A. Bieler, M. Neuland, M. Tulej, and P. Wurz, Performance evaluation of a miniature laser ablation time-of-flight mass spectrometer designed for in situ investigations in planetary space research, *Jou. Mass Spectr.* 48 (2013) 1–15.
- [5] A. Balogh, M. Bird, L. Blomberg, P. Bochsler, J.-L. Bougeret, J. Brückner, L. Iess, J. Guest, Y. Langevin, A. Milani, J.-A. Sauvaud, W. Schmidt, T. Spohn, R. von Steiger, N. Thomas, K. Torkar, H. Wänke and P. Wurz, BepiColombo—An interdisciplinary cornerstone mission to the planet Mercury. ESA-SCI(2000)1, Noordwijk, The Netherlands, European Space Agency (2000).
- [6] A. Riedo, V. Grimaudo, P. Moreno-García, M. Neuland, M. Tulej, P. Broekmann, and P. Wurz, Laser Ablation / Ionisation Mass Spectrometry: Sensitive and quantitative chemical depth profiling of solid materials, *CHIMIA* 70 (2016), 268–273, doi: 10.2533/chimia.2016.268.
- [7] V. Grimaudo, P. Moreno-García, A. Riedo, A. Cedeño López, M. Tulej, R. Wiesendanger, P. Wurz, and P. Broekmann, Review - Laser Ablation Ionization Mass Spectrometry (LIMS) for Analysis of Electrodeposited Cu Interconnects, *Jou. Electrochem. Soc.* 166 (2018), D3190–D3199, DOI: 10.1149/2.0221901jes.
- [8] Riedo, A., M. Neuland, S. Meyer, M. Tulej, and P. Wurz, *J. Anal. Atom. Spectrom.* 28 (2013), 1256–1269.
- [9] R. Wiesendanger, V. Grimaudo, P. Moreno, A. Cedeño López, A. Riedo, M. Tulej, A. Neubeck, M. Ivarsson, D. Wacey, H. Shea and P. Wurz, *Astrobiol.*, 18(8), (2018), 1071–1080.
- [10] Tulej, M., A. Riedo, M.B. Neuland, S. Meyer, D. Lasi, D. Piazza, N. Thomas, and P. Wurz, *Geostand. Geoanal. Res.*, 38 (2014), 441–466.
- [11] A. Riedo, M. Tulej, U. Rohner, and P. Wurz, High-speed strip-line multi-anode Multichannel Plate Detector System, *Rev. Sc. Instr.* 88 (2017), 045114, DOI: 10.1063/1.4981813.

- [12] Grimaudo, V., P. Moreno-García, A. Riedo, M.B. Neuland, M. Tulej, P. Broekmann, and P. Wurz, *Anal. Chem.* 87 (2015), 2037–2041.
- [13] V.A. Azov, L. Mueller, and A.A. Makarov, *Laser Ionization Mass Spectrometry at 55: Quo Vadis?*, *Mass Spectr. Rev.* (2020) 1–55, DOI: 10.1002/mas.21669.
- [14] R. Lukmanov, M. Tulej, R. Wiesendanger, A. Riedo, V. Grimaudo, N. Ligterink, C. de Koning, A. Neubeck, D. Wacey, and P. Wurz, Multi-wavelength ablation/ionisation and mass spectrometric analysis of 1.88 Ga Gunflint Chert, *Astrobiology* (2020), submitted.
- [15] R. Lukmanov, M. Tulej, N.F.W. Ligterink, C. De Koning, A. Riedo, V. Grimaudo, A. Neubeck, D. Wacey, P. Wurz, Chemical identification of microfossils from the 1.88 Ga Gunflint chert. Towards empirical biosignatures with LIMS data, *Proc. Nat. Aca. Sci.* (2020) submitted.
- [16] M. Tulej, A. Neubeck, M. Ivarsson, A. Riedo, M.B. Neuland, S. Meyer, and P. Wurz, Chemical composition of micrometre-sized filaments in an aragonite host by a miniature laser ablation/ionisation mass spectrometer, *Astrobiology* 15(8), (2015a) 669–682, doi: 10.1089/ast.2015.1304.
- [17] M. Tulej, A. Neubeck, A. Riedo, R. Lukmanov, V. Grimaudo, N.F.W. Ligterink, M. Ivarson, W. Bach, C. de Koning, and P. Wurz, Isotope abundance ratio measurements using femtosecond laser ablation ionization mass spectrometry, *Jou. Mass Spectrom.* 55(e4660), (2020), 16 pages, DOI: 10.1002/jms.4660.
- [18] S. Frey, R. Wiesendanger, M. Tulej, M.B. Neuland, A. Riedo, V. Grimaudo, P. Moreno-García, A. Cedeño López, M. Mohos, B. Hofmann, K. Mezger, P. Broekmann, and P. Wurz, Chemical analysis of a lunar meteorite by laser ablation mass spectrometry, *Planet. Sp. Sci.*, 182 (2020) 104816, 6 pages, DOI: 10.1016/j.pss.2019.104816.
- [19] M.B. Neuland, S. Meyer, K. Mezger, A. Riedo, M. Tulej, and P. Wurz, Probing the Allende meteorite with a miniature Laser-Ablation Mass Analyser for space application, *Plan. Sp. Sci.* 101, (2014) 196–209.
- [20] Moreno-García, P., V. Grimaudo, A. Riedo, M. Tulej, M.B. Neuland, P. Wurz, and P. Broekmann, *Electrochim. Acta* 199 (2016), 394–402.
- [21] Grimaudo, V., P. Moreno-García, A. Riedo, S. Meyer, M. Tulej, M.B. Neuland, C. Gütz, S. Waldvogel, P. Wurz, and P. Broekmann, (2017) *Anal. Chem.*, 89, 1632–1641.
- [22] V. Grimaudo, M. Tulej, A. Riedo, R. Lukmanov, N.F. W. Ligterink, C. de Koning, and P. Wurz, (2020) *Rapid Comm. Mass Spectrom.*, 34:e8803 (2020), 11 pages, DOI: 10.1002/rcm.8803.
- [23] A. Cedeño López, V. Grimaudo, A. Riedo, M. Tulej, R. Wiesendanger, R. Lukmanov, P. Moreno-García, E. Lörtscher, P. Wurz, and P. Broekmann, Three-Dimensional Compositional Analysis of SnAg Solder Bumps using Ultraviolet Femtosecond Laser Ablation Ionization Mass Spectrometry, *Anal. Chem.* 92 (2020a), 1355–1362, DOI: 10.1021/acs.analchem.9b04530.
- [24] A. Riedo, S. Meyer, B. Heredia, M.B. Neuland, A. Bieler, M. Tulej I. Leya, M. Iakovleva, K. Mezger and P. Wurz, Highly accurate isotope composition measurements by a miniature laser ablation mass spectrometer designed for in situ investigations on planetary surfaces, *Planet. Space Sci.* 87 (2013), 1–13.
- [25] S. Maurice, R.C. Wiens, M. Saccoccio, B. Barraclough, O. Gasnault, O. Forni, N. Mangold, D. Baratoux, S. Bender, G. Berger, J. Bernardin, M. Berthé, N. Bridges, D. Blaney, M. Bouyé, P. Caïs, B. Clark, S. Clegg, A. Cousin, D. Cremers, A. Cros, L. DeFlores, C. Derycke, B. Dingler, G. Dromart, B. Dubois, M. Dupieux, E. Durand, L. d’Uston, C. Fabre, B. Faure, A. Gaboriaud, T. Gharsa, K. Herkenhoff, E. Kan, L. Kirkland, D. Kouach, J.-L. Lacour, Y. Langevin, J. Lasue, S. Le Mouélic, M. Lescure, E. Lewin, D. Limonadi, G. Manhès, P. Mauchien, C. McKay, P.-Y. Meslin, Y. Michel, E. Miller, H.E. Newsom, G. Ortner, A. Paillet, L. Parès, Y. Parot, R. Pérez, P. Pinet, F. Poitrasson, B. Quartier, B. Sallé, C. Sotin, V. Sautter, H. Séran, J.J. Simmonds, J.-B. Sirven, R. Stiglich, N. Striebig, J.-J. Thocaven, M.J. Toplis, D. Vaniman, The ChemCam Instrument Suite on the Mars Science Laboratory (MSL) Rover: Science Objectives and Mast Unit Description, *Sp. Sci Rev.* 170(1–4), (2012) 95–166, DOI: 10.1007/s11214-012-9912-2
- [26] R.C. Wiens, S. Maurice, B. Barraclough, M. Saccoccio, W.C. Barkley, J.F. Bell III, S. Bender, J. Bernardin, D. Blaney, J. Blank, M. Bouyé, N. Bridges, N. Bultman, P. Caïs, R.C. Clanton, B. Clark, S.Clegg, A. Cousin, D. Cremers, A. Cros, L. DeFlores, D. Delapp, R. Dingler, C. D’Uston, M. Darby Dyar, T. Elliott, D. Enemark, C. Fabre, M. Flores, O. Forni, O. Gasnault, T. Hale, C. Hays, K. Herkenhoff, E. Kan, L. Kirkland, D. Kouach, D. Landis, Y. Langevin, N. Lanza, F. LaRocca, J. Lasue, J. Latino, D. Limonadi, C. Lindensmith, C. Little, N. Mangold, G. Manhes, P. Mauchien, C. McKay, E. Miller, J. Mooney, R.V. Morris, L. Morrison, T. Nelson, H. Newsom, A. Ollila, M. Ott, L. Pares, R. Perez, Fr. Poitrasson, C. Provost, J.W. Reiter, T. Roberts, F. Romero, V. Sautter, S. Salazar, J.J. Simmonds, R. Stiglich, S. Storms, N. Striebig, J.-J. Thocaven, T. Trujillo, M. Ulibarri, D. Vaniman, N. Warner, R. Waterbury, R. Whitaker, J. Witt, B. Wong-Swanson, The ChemCam Instrument Suite on the Mars Science Laboratory (MSL) Rover: Body Unit and Combined System Tests, *Space Sci. Rev.*, 170, (2012) 167–227, DOI: 10.1007/s11214-012-9902-4

- [27] R. Gellert, J.L. Campbell, P.L. King, L.A. Leshin, G.W. Lugmair, J.G. Spray, S.W. Squyres, A.S. Yen, The Alpha-Particle-X-ray-Spectrometer (APXS) for the Mars Science Laboratory (MSL) Rover Mission, LPSC (2009), abstract nr.: 2364
- [28] Moreno-García, P., V. Grimaudo, A. Riedo, M. Tulej, P. Wurz, and P. Broekmann, *Rapid Commun. Mass Spectrom.*, 30 (8), (2016a) 1031–1036.
- [29] Neuland, M.B., K. Mezger, A. Riedo, M. Tulej, and P. Wurz, (2016), *Meas. Sci. Technol.*, 27(3), 035904.
- [30] M. Tulej, R. Lukmanov, V. Grimaudo, A. Riedo, C. de Koning, N.F.W. Ligterink, A. Neubeck, M. Ivarson, and P. Wurz, Determination of the microscopic mineralogy of inclusion in an amygdaloidal pillow basalt by fs-LIMS, *Jou. Anal. At. Spectrom.* (2020), in press.
- [31] S.F. Anderson, K. Nowicki, and T. Whitaker, In-Situ Rb-Sr Geochronology, IEEE Aerospace Conf., 1–8, (2013) doi: 10.1109/AERO.2013.6497158.
- [32] B. A. Cohen, Development of the Potassium-Argon Laser Experiment (KARLE) Instrument for in situ Geochronology, 43rd Lunar and Planetary Science Conference (2012), abstract # 1267.
- [33] D.L. Talboys, S.Barber, J.C. Bridges, S.P. Kelley, D. Pullan, A.B. Verchovsky, G. Butcher, A. Fazel, G.W. Fraser, C.T. Pillinger, M.R. Sims, I.P. Wright, In situ radiometric dating on Mars: Investigation of the feasibility of K-Ar dating using flight-type mass and X-ray spectrometers, *Plan. Sp. Sci.* 57 (2009) 1237–1245.
- [34] K.A. Farley, C. Malespin, P. Mahaffy, J.P. Grotzinger, P.M. Vasconcelos, R.E. Milliken, M. Malin, K.S. Edgett, A.A. Pavlov, J.A. Hurowitz, J.A. Grant, H.B. Miller, R. Arvidson, L. Beegle, F. Calef, P.G. Conrad, W.E. Dietrich, J. Eigenbrode, R. Gellert, S. Gupta, V. Hamilton, D.M. Hassler, K.W. Lewis, S.M. McLennan, D. Ming, R. Navarro-González, S.P. Schwenzer, A. Steele, E.M. Stolper, D.Y. Sumner, D. Vaniman, A. Vasavada, K. Williford, R.F. Wimmer-Schweingruber, the MSL Science Team, In Situ Radiometric and Exposure Age Dating of the Martian Surface, *Science* 343 (2014) 1247166, 5 pages, DOI: 10.1126/science.1247166
- [35] B.J.A. Willigers, J.A. Baker, E.J. Krostad, and D.W. Peate, Precise and accurate in situ Pb–Pb dating of apatite, monazite, and sphene by laser ablation multiple-collector ICP-MS, *Geochimica et Cosmochimica Acta* 66, (2002) 1051–1066
- [36] Tatsumoto, M., and J. N. Rosholt, Age of the Moon: An Isotopic Study of Uranium-Thorium-Lead Systematics of Lunar Samples, *Science*, 167 (1970), 461-463, DOI: 10.1126/science.167.3918.461
- [37] A.A. Nemchin, R.T. Pidgeon, M.J. Whitehouse, J.P. Vaughan, C. Meyer, SIMS U–Pb study of zircon from Apollo 14 and 17 breccias: implications for the evolution of lunar KREEP, *Geochimica et Cosmochimica Acta* 72, (2008) 668–689
- [38] W. Bach, M. Rosner, N. Jons, S. Rausch, L.F. Robinson, H. Paulick, and J. Erzinger, Carbonate veins trace seawater circulation during exhumation and uplift of mantle rock: Results from ODP Leg 209, *Earth Plan. Sci. Lett.* 311, (2011) 242–252
- [39] G. Ratié, D. Jouvin, J. Garnier, O. Rouxel, S. Miska, E. Guimarães, L. Cruz Vieira, Y. Sivry, I. Zelano, E. Montarges-Pelletier, F. Thil, and C. Quantin, Nickel isotope fractionation during tropical weathering of ultramafic rocks, *Chem. Geol.* 402 (2015), 68–76, DOI: 10.1016/j.chemgeo.2015.02.039.
- [40] Riedo, A., V. Grimaudo, P. Moreno-García, M.B. Neuland, M. Tulej, P. Wurz, and P. Broekmann, *J. Anal. At. Spectrom.* 30 (2015), 2371–2374.
- [41] M. Tulej, R. Wiesendanger, A. Riedo, G. Knopp, and P. Wurz, Mass spectrometric analysis of Mg-plasma produced by double-pulse femtosecond laser irradiation, *Jou. Anal. At. Spec.* 33 (2018), 1292-1303, DOI: 10.1039/C8JA00036K.
- [42] D. Käser, L. Hendriks J. Koch and D. Günther, Depth profile analyses with sub 100-nm depth resolution of a metal thin film by femtosecond - laser ablation - inductively coupled plasma - time-of-flight mass spectrometry. *Spectrochimica Acta Part B: Atomic Spectroscopy*, 149 (2018), 176–183.
- [43] A. Riedo, V. Grimaudo, A. Cedeño López, M. Tulej, P. Wurz, and P. Broekmann, Novel 2D binning approach for advanced LIMS depth profiling analysis, *Jou. Anal. At. Spectrom.* 34 (2019), 1564-1570, doi: 10.1039/C9JA00138G.
- [44] P. Wurz, D. Abplanalp, M. Tulej, M. Iakovleva, V.A. Fernandes, A. Chumikov, and G. Managadze, Mass Spectrometric Analysis in Planetary Science: Investigation of the Surface and the Atmosphere, *Sol. Sys. Res.* 46, (2012) 442–459
- [45] R.A. Kerr, Hayabusa Gets to the Bottom of Deceptive Asteroid Cloaking, *Science* 333, (2011) 1081
- [46] T. Noguchi, T. Nakamura, M. Kimura, M.E. Zolensky, M. Tanaka, T. Hashimoto, M. Konno, A. Nakato, T. Ogami, A. Fujimura, M. Abe, T. Yada, T. Mukai, M. Ueno, T. Okada, K. Shirai, Y. Ishibashi, and R. Okazaki, Incipient Space Weathering Observed on the Surface of Itokawa Dust Particles, *Science* 333, (2011) 1121–1125, DOI: 10.1126/science.1207794.

- [47] T. Nakamura, T., T. Noguchi, M. Tanaka, M.E. Zolensky, M. Kimura, A. Tsuchiyama, A. Nakato, T. Ogami, H. Ishida, M. Uesugi, T. Yada, K. Shirai, A. Fujimura, R. Okazaki, S.A. Sandford, Y. Ishibashi, M. Abe, T. Okada, M. Ueno, T. Mukai, M. Yoshikawa, and J. Kawaguchi, Itokawa Dust Particles: A Direct Link Between S-Type Asteroids and Ordinary Chondrites, *Science* 333, (2011) 1113–1116
- [48] C.M. Pieters, L.A. Taylor, S.K. Noble, L.P. Keller, B. Hapke, R.V. Morris, C.C. Allen, D.S. McKay, and S. Wentworth, Space weathering on airless bodies: Resolving a mystery with lunar samples. *Meteoritics & Planetary Science*, 35 (2000), 1101–1107. doi: 10.1111/j.1945-5100.2000.tb01496.x
- [49] L.P. Keller and D.S. McKay, Discovery of Vapor Deposits in the Lunar Regolith, *Science* 261(93), (1993) 1305–1307
- [50] M.B. Neuland, K. Mezger, A. Riedo, M. Tulej, and P. Wurz, Quantitative measurement of the chemical composition of geological standards with a miniature laser ablation/ionisation mass spectrometer designed for in situ application in space research, *Meas. Tech.*, 27(3), (2016) 035904, DOI: 10.1088/0957-0233/27/3/035904.
- [51] E. Gnos, B.A. Hofmann, A. Al-Kathiri, S. Lorenzetti, O. Eugster, M.J. Whitehouse, I.M. Villa, A.J.T. Jull, J. Eikenberg, B. Spettel, U. Krähenbühl, I.A. Franchi, and R.C. Greenwood, Pinpointing the Source of a Lunar Meteorite: Implications for the Evolution of the Moon, *Science* 305 (2004), 657–659.
- [52] A. Riedo and P. Wurz, Laser Ablation Ionisation Mass Spectrometry on the Lunar Surface for the Artemis Mission, Federal Department of Economic Affairs, Education and Research, EAER, 2020, Switzerland.

## BIOGRAPHY



**Peter Wurz** has a degree in electronic engineering (1985), an M.Sc. and a Ph.D. in Physics from Technical University of Vienna, Austria (1990). He has been a post-doctoral researcher at Argonne National Laboratory, USA. Since 1992 at the University of Bern. He is a Professor of physics and since 2015 head of the Space Science and Planetology division. He has been Co-I and PI for many science instruments for space missions of ESA, NASA, ISRO, CNSA, Roscosmos, and JAXA.



**Marek Tulej** received a Ph.D. in Physical Chemistry from the University of Basel, Switzerland in 1999. After his post-doctoral period at Paul Scherrer Institute (PSI), Switzerland, he joined in 2008 the University of Bern as an instrument scientist for space missions, including Phobos-Grunt, Marco Polo-R, Luna-Resurs, and JUICE.



**Andreas Riedo** received his Ph.D. in Physics in 2014 from the University of Bern, Switzerland. In 2016 he received a SNSF fellowship that allowed him to continue his research in Astrobiology at the Leiden University, The Netherlands. He extended his stay at the Leiden University with a MCSA fellowship for another two years before he moved in 2019 to the Free University Berlin after receiving the prestigious Einstein fellowship. In 2020 he moved to University of Bern and is currently appointed as researcher and project manager within the JUICE space mission.



**Valentine Grimaudo** received a Ph.D in Chemistry and Molecular Sciences from the University of Bern, Switzerland, in 2018, where she developed new measurement procedures based on LIMS for the chemical analysis of industrial process in the interconnect technology. After her degree she joined the Space Science and Planetology division at the University of Bern as post-doctoral researcher.



**Rustam Lukmanov** did a BSc and a MSc in Geology, St.-Petersburg State University, Russia, where he worked on Microanalytical studies of the iron oxidation state in mantle spinels. Since 2017 he is at the University of Bern, working on his PhD by the investigation fossils in minerals to characterize early life with the LIMS instrument.



*Nicolas Thomas has MSc. in Experimental Space Physics" from the University of Leicester (1982), and a PhD in Physics University of York (1986). PostDoc at Max-Planck-Institut für Aeronomie (MPAe) working on the Halley Multicolour Camera of the Giotto mission (ESA), PostDoc at ESA (1991-1992), MPAe staff (1992–2003), and since then professor at University of Bern. He has been Co-I and PI for many science instruments for space missions. Currently he is PI of the CaSSIS camera on the ExoMars mission (ESA).*